Revealing polymerisation defects and formation mechanisms in aldol condensation for conjugated polymers via high-resolution molecular imaging

Xiaocui Wu,[1] Stefania Moro,[2] Adam Marks,[3,4] Maryam Alsufyani,[3] Zidi Yu,[5] Luís M.A. Perdigão,[1] Xingxing Chen,[3,6] Alexander M. T. Luci,[1] Callum Crockford,[1] Simon E.F. Spencer[7], David J. Fox,[1] Jian Pei,[5] Iain McCulloch,[3] Giovanni Costantini[2*]

[1]Department of Chemistry, University of Warwick, Coventry, CV4 7AL, United Kingdom

[2]School of Chemistry, University of Birmingham, Birmingham, B15 2TT, United Kingdom

[3]Department of Chemistry, University of Oxford, Oxford, OX1 3TA, United Kingdom

[4]Department of Materials Science and Engineering, Stanford University, California, 94305, United States

[5]College of Chemistry and Molecular Engineering, Peking University, Beijing, 100871, China

[6]Department of Materials, School of Chemistry & Chemical Engineering, Anhui University, Hefei, 230601, Anhui, China

[7]Department of Statistics, University of Warwick, Coventry, CV4 7AL, United Kingdom

*Email: g.costantini@bham.ac.uk

KEYWORDS: aldol condensation, conjugated polymers, scanning tunnelling microscopy, polymerisation defects, reaction mechanism.

Abstract

Aldol condensation is a crucial synthetic reaction in organic chemistry, particularly valued for fabricating conjugated polymers without the use of metals or toxic organostannanes. However, due to the lack of reliable and precise analytical methods, no direct evidence of the microstructure and sequence of synthesised polymers has been obtained, limiting control over their structure and performance. Here, by combining electrospray deposition and scanning tunnelling microscopy (ESD-STM), we analyse sub-monomer resolution images of four different *n*-type polymers produced via aldol condensation, revealing unexpected defects in both the sequence of (co)monomers and their coupling. These defects, observed across all polymer samples, indicate alternative side reaction pathways inherent to aldol condensation, affecting both polymerisation and small-molecule reactions. Our findings not only uncover the reaction mechanism responsible for these defects but also bring new insights for the design of more effective synthetic pathways to minimise structural defects in conjugated polymers.

Conjugated polymers (CPs) present numerous advantages such as low cost, lightweight, mechanical flexibility and solution processability, making them particularly appealing materials for applications in opto-electronics, (bio)sensors, organic light emitting diodes (OLEDs), organic field-effect transistors (OFETs), neuromorphic computing and energy storage[1,2]. Since the report of poly(p-phenylene vinylene) for large-area OLED devices[3], a variety of CPs have been proposed and fabricated over the past 30 years with complex chemical compositions and structures typically obtained through multi-step co-polymerisation techniques[4,5]. Cross-coupling polycondensation reactions catalysed by transition metals are commonly employed to synthesise CPs, including Suzuki-Miyaura[6,7], Mizoroki–Heck[8,9], Sonogashira[10], Kumada[11] and Stille polymerisation[12]. However, they often require the use of precious metals as catalysts, making them impractical for large-scale industrial use. As a consequence, more economical and environmentally friendlier alternatives have been sought after. Among these aldol condensation, one of the most versatile synthetic methods employed in organic chemistry[13], has attracted significant attention[14,15].

Aldol condensation involves the nucleophilic addition of a ketone enolate to an aldehyde or ketone. By losing a water molecule, which is the only by-product of the reaction, the initially formed β-hydroxycarbonyl compound is transformed into an α,β-unsaturated carbonyl species, which can then be extracted from the solution without laborious purification steps[16,17]. In contrast to the well-developed cross-coupling polycondensations, the aldol reaction does not require metal catalysts which have been shown to often remain as residual impurities in the conjugated polymers and to affect their efficiency[18,19,20]. Moreover, aldol condensation affords rigid backbones due to the formation of double C=C bonds, thereby eliminating single-bond rotation and imparting a coplanar conjugated backbone, which is known to promote charge delocalization and efficient charge transport[15]. Thus, it is emerging as a greener and cheaper approach to synthesise semiconducting polymers, in particular *n*-type materials[15,20,21,22,23,24]. However, limited information is available on the quality of the resulting materials, i.e. the precise chemical structure of the synthesised polymers in terms of their sequence and the potential presence of polymerisation defects, which are known to possibly affect the performance of CP-based devices[25,26,27,28,29].

There is therefore a rising demand for the precise and reliable characterisation of these functional materials, in particular of their exact sequence, which also allows for an improved understanding of the polymerisation mechanism and, ultimately, for a better, molecular-scale control of the

synthesised materials. Traditional characterisation techniques such as nuclear magnetic resonance (NMR), mass spectrometry (MS) or size exclusion chromatography (SEC) are not ideal to analyse CPs given their low solubility, high tendency to aggregation, low volatility in MS and the lack of reliable calibration standards in SEC. Recently, the combination of electrospray deposition (ESD) with scanning tunnelling microscopy (STM) made it possible to determine the exact sequence and mass distribution of the polymers, including the presence of possible polymerisation defects[25,30,31,32,33] as well as to establish the assembly patterns with molecular scale insight[34,35,36,37].

This methodology has been particularly useful in analysing the structure of the fused rigid-rod polymer **1** (Fig. 1a) which is synthesised via aldol condensation and shows excellent environmental stability in OFET devices[38]. Besides demonstrating that this polymer has an unusually high persistence length, the ESD-STM characterisation also revealed the presence of kinks in the overall straight backbones, which were tentatively attributed to *cis*-defects in the double bond linkage between the monomers[35]. A simple statistical analysis of these kinks reveals that they are rather frequent, corresponding to about 9% of all monomer linkages (see section 3.2 of the Supplementary Information, SI). Because of the high rotational rigidity of double C=C bonds at room temperature, these kinks cannot result from conformational disorder but must be intrinsic structural defects arising from the way monomers have coupled during the polymerisation. Our preliminary investigations of **1** thus prompt a thorough reassessment of the conventional reaction mechanism typically assumed for aldol condensation.

To this aim, here we study four structurally different *n*-type co-polymers of increasing complexity (Figs. 1b-1e) – all involving aldol condensation reactions. Specifically, while aldol condensation is used as the polymerisation reaction for copolymers 2, 3 and 4, in the case of copolymer 5, aldol condensation is only employed to synthesise one of the two comonomers, which are subsequently polymerised through a Stille reaction. The ESD-STM analysis clearly identifies and quantifies the appearance of two types of unexpected polymerisation defects: deviations from the ideal polymer sequence, resulting from the wrong ordering of comonomers (*sequence defects*), and kinks in the backbone structure, resulting from their incorrect coupling position or orientation (*coupling defects*). Based on the experimental results, detailed reaction pathways leading to the formation of the observed defects are proposed, bringing new insight into the mechanism of the aldol condensation reaction.

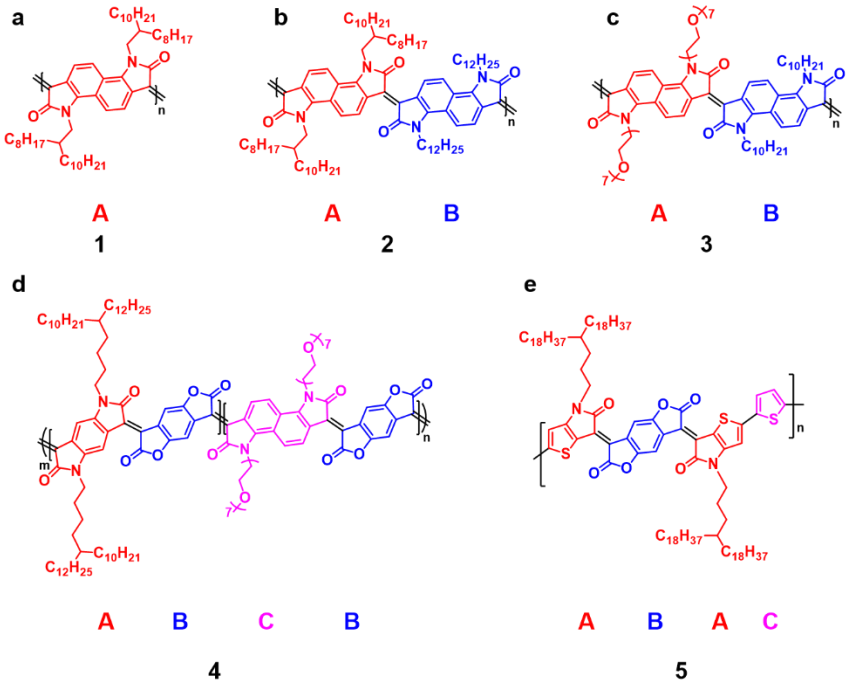

Fig. 1: Chemical structures of the conjugated polymers studied in this work. The comonomers of each polymer are marked in a different colour and labelled with a different letter. The generic aldol condensation steps involved in the synthesis of polymers **1**-**5** are shown in Scheme S1.

Results and discussion

The first step in our study was to move from homopolymer **1** by increasing its complexity while also exploring the potential role of bulky side chains in influencing the occurrence of coupling defects. To this aim, we synthesised co-polymer **2** (see Fig. 1b), which has a branched $C_2C_{8;10}$ (with C_2 being the linker to the branched $C_{8;10}$ side chain) and a linear C_{12} alkyl side chain tethered to the bis-oxindole monomer units (Fig. 1b). Effectively, **2** is obtained from **1** by replacing every second $C_2C_{8;10}$ branched side chain with a less bulky linear C_{12} chain.

Figure 2 shows STM images acquired after the room temperature ESD of **2** onto a pristine Au(111) surface. In high molecular coverage areas, the polymers form relatively compact monolayers where individual molecules tend to align mostly parallel to each other (Fig. 2a). Individual polymers (Fig. 2c and Fig. S3a) have straight backbones (grey stripe in Fig. S3b) surrounded on both sides by alternating larger and smaller oval-shaped bright dots (red and blue in Fig. S3b,

respectively), and by dimmer elongated features emerging almost perpendicularly from these dots. These are identified as the side chains, with the larger dots corresponding to the starting points of the branched $C_2C_{8;10}$ alkyl side chains, and the smaller ones representing the starting points of the linear C_{12} side chains.

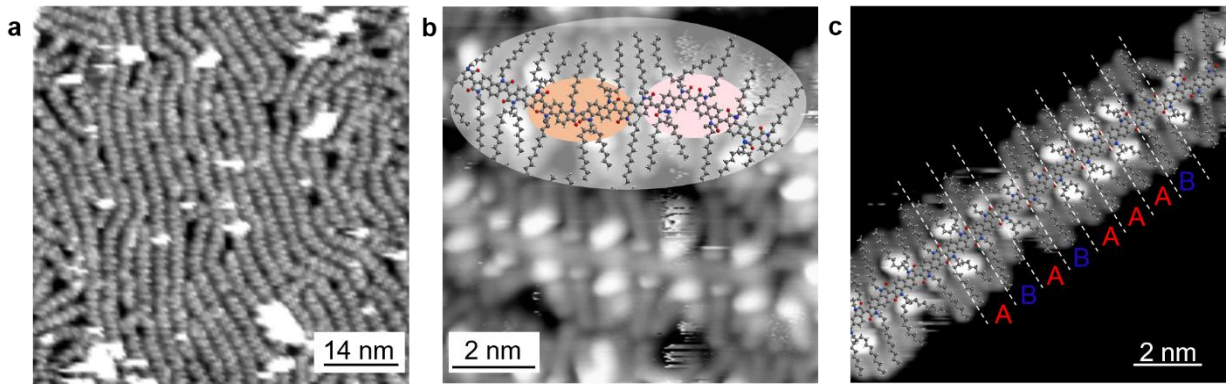

Fig. 2: STM characterisation of polymer 2. a, Large-scale STM image of copolymer **2** acquired in a high coverage area (70 nm × 70 nm, V = 950 mV, I = 78 pA). **b,** High-resolution STM image of a high coverage area (10 nm × 10 nm, V = 51 mV, I = 90 pA) showing coupling defects. Pink and orange ovals highlight different types of kinks in the polymer backbone and correspond to c2 and c3 defects, respectively, as illustrated in Fig. 3a. **c,** High-resolution STM image of an isolated polymer showing sequence defects (10 nm × 10 nm, V = 149 mV, I = 120 pA). Scaled molecular models of the polymer are superimposed on the upper part of image (b) and on image (c).

While the backbones of **2** are mostly straight, occasional kinks can be seen in the STM images (*e.g.*, see pink and orange ovals in Fig. 2b and Fig. S4), similarly to what had been observed for **1**[35]. In order to determine the precise molecular structure of the polymers in correspondence to these kinks, we fitted geometry-optimised molecular models of **2** onto a large number of STM images (*e.g.*, Fig. 2b), making sure that all features in the images were correctly accounted for, in particular the positions, orientations and starting points of the side chains (see section 3.1 of the SI for a detailed explanation of the fitting process). By doing so, we were able to identify several types of coupling between the A and B comonomers, differing from those typically expected in aldol condensation reactions, offering a potential explanation for the origin of the observed kinks (Fig. 3a).

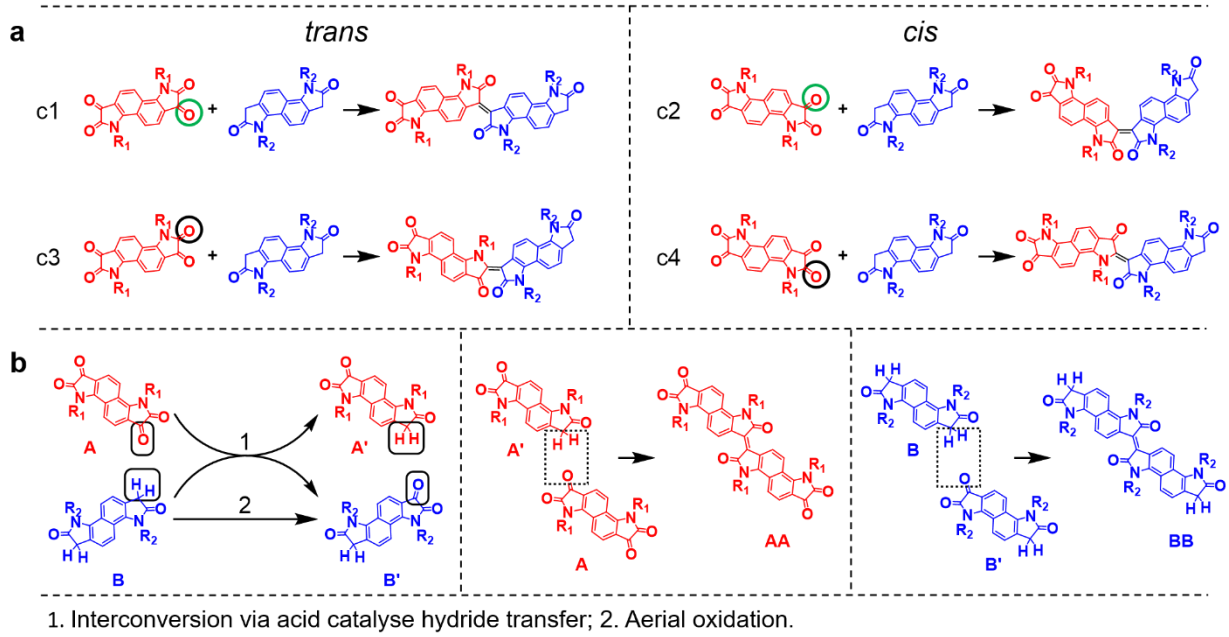

Fig. 3: Possible reaction pathways for coupling and sequence defects between two isatin-based comonomers. a, Coupling defects. Reactions c2-c4 lead to the formation of kinks in the polymer backbone, with progressively shallower angles. The carbonyls β and α to the nitrogen atom of the pyrrole ring, where the reaction takes place, are circled in green and black, respectively. **b,** Possible reaction pathways leading to AA and BB polymer sequence defects. A and B comonomers are marked in red and blue, respectively.

The most frequently observed coupling (as reported in Table 1) is c1 in Fig. 3a, where the carbonyl β to the nitrogen in the A comonomer (circled in green in Fig. 3a) reacts with the oxindole hydrogen of the B comonomer. This *trans* coupling is what is usually expected in the aldol condensation reaction and results in a straight polymer backbone. However, the same two comonomers could potentially also react in the c2 *cis* coupling geometry in Fig. 3a. This latter reaction is expected to be less favourable than c1 because of the steric repulsion from the close proximity of the two carbonyls in the final product, which causes a kink of about 130° in the polymer backbone (Fig. S5). The c2 *cis* backbone configurations are indeed observed in the STM images (*e.g.*, see pink oval in Fig. 2b and Fig. S4a) although much less frequently than the straight *trans* configurations (see Table 1). Very similar kinks were also observed for **1**[35] (see also Fig. S2), so we expect them to be caused by the same type of c2 *cis* coupling.

Table 1 Backbone defect frequencies for polymers 2 and 3.

	Coupling	2		3	
		Count	Frequency	Count	Frequency
Defects	c2	19	2.6%	20	3.6%
	c3	12	1.7%	4	0.7%
	c4	0	0.0%	2	0.4%
	Sum	31	**4.3%**	26	**4.7%**
	c1	687	**95.7%**	525	**95.3%**

	Sequence	2		3	
		Count	Frequency	Count	Frequency
Defects	AA	10	**1.4%**	16	**2.9%**
	BB	15	**2.1%**	66	**12.0%**
	Sum	25	**3.5%**	82	**14.9%**
	AB	693	**96.5%**	469	**85.1%**

Monomer	2			3		
	Count		Frequency	Count		Frequency
A	436	845	**51.6%**	327	694	**47.1%**
B	409		**48.4%**	367		**52.9%**

While c1 is the correct *trans* coupling, c2-c4 are defective couplings, as illustrated in Fig. 3a. The relative frequencies were calculated with respect to the total amount of analysed coupling configurations (left) and sequence configurations (right). The corresponding 95% confidence intervals are reported in Table S1.

The bis-isatin A comonomer of **2** has two carbonyl groups. The reactivity of the carbonyl β to the nitrogen atom (circled in green in Fig. 3a) is expected to be higher due to a combination of steric and electron density arguments. In fact, the β carbonyl is more susceptible to attack from the enolate which is formed upon deprotonation of the acidic α hydrogen on the oxindole monomer. However, it cannot *a priori* be excluded that also the carbonyl α to the nitrogen atom (circled in black in Fig. 3a) may react with the oxindole hydrogen of the B comonomer. Moreover, for this reaction both *trans* and a *cis* configurations are possible, resulting in the two further coupling schemes c3 and c4 in Fig. 3a, respectively. Based on simple molecular models, the backbone configurations resulting from c3 and c4 are expected to show fewer sharp kinks of about 150° and 175°, respectively (Fig. S5). In the STM images only very few cases of c3 couplings could be identified (*e.g.*, see orange ovals in Fig. 2b and Fig. S4b), while no c4 coupling could be observed.

While polymer **2** is mostly characterised by an alternating $(AB)_n$ sequence where the side chains in consecutive comonomers are different, the analysis of the STM images also identified several cases where two (or even more) identical side chains are located in successive positions on both

sides of the backbone. An example can be found in Fig. 2c, showing an isolated polymer strand where the otherwise alternating sequence of A and B comonomers is interrupted by three successive A units in its upper right section. Another example is given in Fig. S6, displaying a case of two successive B units.

These configurations cannot result from direct homocouplings between the A and B comonomers: in fact, the A comonomer cannot couple to itself by aldol condensation, while a *trans* BB homocoupling would create a noticeable kink in the polymer backbone (Fig. S7); a *cis* BB homocoupling would cause a much shallower kink but would also have two successive side chains on the same side of the backbone (Fig. S7). Neither kinks nor same-side side chains were ever observed in the case of successive identical side chains. On the contrary, AA and BB polymer sequences were always seen to occur in straight segments of the backbone, indicating that they are resulting from a "regular" c1 coupling. Thus, these sequence defects are likely the consequence of a different reaction mechanism. One possibility is for the CH_2 in A and the C=O in B to exchange positions in an acid catalysed hydride transfer reaction[39] producing A' and B' thus allowing the formation of both AA and BB units in the polymer (Fig. 3b). The proposed mechanism of this interconversion is shown in section 2 of the SI. In addition, it is also possible to oxidise (via aerial oxidation during the aldol reaction) the CH_2 in monomer B to a C=O, forming B', allowing its combination with a non-oxidized B to give a BB unit (Fig. 3b). This additional potential pathway is likely the underlying reason for the higher frequency of BB compared to AA defects (Table 1).

In order to check generality of the different reaction pathways identified for **2** and to gauge the influence of the side chain chemistry on these reaction mechanisms, we analysed **3** (Fig. 1c), obtained by replacing the branched hydrophobic alkyl side chain of **2** with a linear hydrophilic 7-unit ethylene glycol (EG) chain, henceforth identified as g_7. This polymer was also made by aldol condensation and shows high electron mobility in organic electrochemical transistors (OECTs)[40].

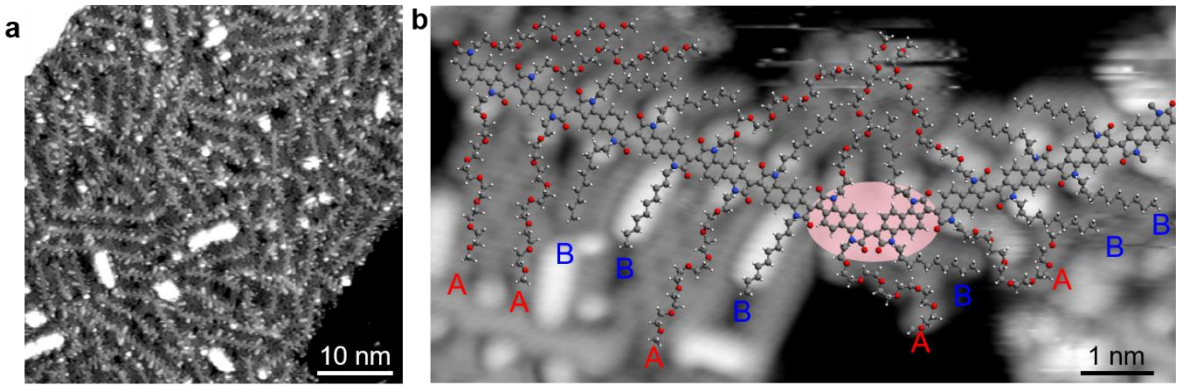

Fig. 4: STM characterisation of polymer 3. a, Large-scale STM image (50 nm × 50 nm, V = 950 mV, I = 110 pA) of copolymer **3**. **b,** High-resolution STM image showing defects in the polymer sequence and backbone structure (5 nm × 10 nm, V = 247 mV, I = 140 pA). The kink in the backbone is marked by a pink oval and corresponds to a c2 (*cis*) coupling (less frequent cases of c3 and c4 couplings are shown in Fig. S8). A geometry-optimised molecular model of the polymer is overlayed on the image in (b).

Figure 4a shows that polymer **3** self-assembles into extended compact islands which, despite being less ordered than those of **2**, still present local parallel packing. Close-up images (Fig. 4b) allow to identify a characteristic sub-structure with bright alternating smaller ovals and larger dumbbell features on both sides of the backbones (highlighted in blue and red, respectively, in Fig. S9b). Shorter linear structures (blue lines in Fig. S9b) extend from the smaller dots and are associated with C_{10} alkyl chains, while longer serpentine features (red lines in Fig. S9b) emerge from the dumbbells and are assigned to the g_7 EG side chains.

Figure 4b demonstrates that, also for **3,** coupling and sequence defects can be identified in the STM images, resulting in kinked backbones and in occasional AA and BB sequences. As in the case of **2**, the sequence defects occur only in straight segments of the backbone, excluding the possibility of homocouplings, but instead pointing to the effective exchange of functional groups between comonomers as proposed in Fig. 3b. Moreover, fitting the STM images of **3** in correspondence to the kinks, reveals the presence of the "incorrect" couplings c2, c3 and c4 shown in Fig. 3a (Fig. S8).

Since **2** and **3** exhibit similar polymerisation defects, it raises the question of whether their side chain chemistry affects the kinetics of the aldol condensation reaction, potentially altering the occurrence of defects. To address this, a statistical analysis of backbone defects was conducted for both polymers and are summarised in Table 1.

The results show that polymers **2** and **3** have a similar amount of coupling defects, with a total percentage of "incorrect" couplings (c2, c3 and c4 in Fig. 3a) of 4-5%, with c2 being the predominant defective coupling. Thus, these sets of data demonstrate experimentally that the different side chains of **2** and **3** do not significantly alter the relative reactivity of the two carbonyls in the A bis-isatin comonomers or the relative probability of *cis* or *trans* couplings. This outcome is somewhat anticipated because, although the oxygen atoms in the EG side chains of **3** might have the potential to affect the electronics/acidity of the carbonyl groups at the α and β positions in the bis-isatin monomer, they are situated at a considerable distance. Additionally, the steric hindrance that impairs the defective couplings is mostly independent of the side chains in c2 and c3, and just dependent on the presence of a side chain in c4, rather than on its specific chemical nature.

However, an obvious difference is observed when it comes to the sequence defects. In fact, while for **2** only a limited amount of sequence defects is detected (with 1% of AA and 2% of BB sequences, see Table 1), these are much more frequent for **3** (with 3% of AA and 12% of BB sequences). It is important to notice that, for both polymers, the total relative amounts of the two comonomers observed in the STM images is very close to the expected value of 1:1, confirming that the correct relative stoichiometry was used for the polymer synthesis. The reported difference seems therefore to be intrinsic to the aldol condensation reaction and suggests a marked influence of the side chain chemistry on the kinetics of the reactions described in Fig. 3b.

To further our analysis of how different chemical and structural parameters influence the generation of synthetic defects during aldol condensation polymerisation, we decided to study **4**, a recently proposed lactone-based rigid semiconducting polymer[24], whose synthesis involves also a third, lactone-based comonomer without side chains (Fig. 1d). Thus, **4** is characterised by a different chemistry of the backbone, by a lower side chain attachment density with respect to **2** and **3** and by longer and more flexible branched alkyl side chains when compared with **1** and **2**.

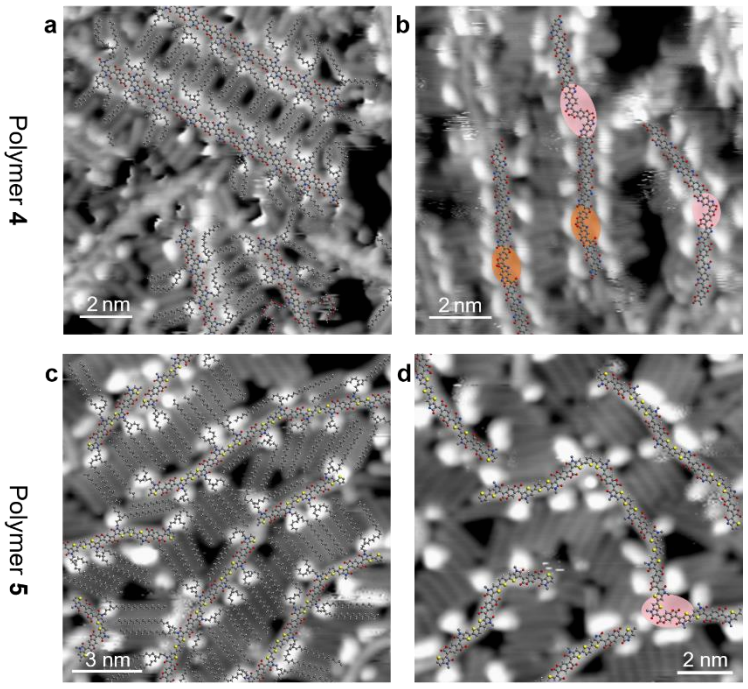

Fig. 5: STM characterisation of polymer 4 and 5. a, Sequence of polymer **4** with predominant AB coupling (15 nm × 15 nm, V = 573 mV, I = 78 pA). **b,** Formation of kinks in the backbone (10 nm × 10 nm, V = 176 mV, I = 90 pA). Pink and orange ovals correspond to c2 and c3 coupling defects, respectively, as illustrated in Fig. S10 and Fig. S11. **c,** High-resolution STM images of polymer **5** (13 nm × 13 nm, V = 247 mV, I = 140 pA). **d**, Formation of kinks in the backbone (10 nm × 10 nm, V = 247 mV, I = 140 pA). The pink oval corresponds to a c2 defect (see Fig. S15). Geometry-optimised molecular models are superposed onto images in (a) and (c), while those of only the backbone are superposed onto images in (b) and (d) to help visualise the kinks.

High-resolution STM images (Fig. 5a and Fig. S12) show that most alkyl branched side chains – $C_{10;12}$ with linear C_5 spacers (red lines in Fig. S12d) – are attached to the polymer backbones, with only a few cases of EG g_7 side chains (magenta lines in Fig. S12d). Thus, the ESD-STM analysis demonstrates that the structure of **4** is not the expected $(AB)_m(CB)_n$ sequence (Fig. 1d) but, mostly, an alternating $(AB)_n$ sequence, which is probably due to the higher solubility of the A comonomer with respect to C in toluene (see section 4 of SI).

The occurrence of occasional kinks is also observed in the backbones of **4** (pink and orange ovals in Fig. 5b). These correspond to coupling defects between both AB and BC pairs of comonomers,

resulting from two different sets of possible reaction pathways (Figs. S10 and S11, respectively), which are the isatin-lactone equivalents of the isatin-isatin reactions shown in Fig. 3a. Examples of c2 and c3 couplings, observed both between AB and BC comonomers, are shown in Fig. S14, while c4 couplings were only observed between AB comonomers. A quantitative analysis of the coupling defects reveals a total frequency of 3.7% (Table S2), which is comparable to those obtained for **2** and **3** (Table 1). This confirms our previous finding that the relative reactivity of the two carbonyls in the bis-isatin-based comonomer does not depend significantly on the chemical nature or, in this case, on the absence of its side chains, nor on whether the isatin monomer is reacting with another isatin-based or with an oxindole-based comonomer. Finally, we note that **4** cannot develop any of the sequence defects as those observed for **2** and **3**, because for **4** the aldol condensation occurs between an isatin-based and an oxindole-based comonomer and thus the effective comonomer exchange reactions described in Fig. 3b cannot take place. No such type of defect was in fact observed in the STM images.

In a final effort to explore the generality of our findings about defects in the aldol condensation, a final polymer, **5**[41,42,43], was analysed. Its synthesis involves both an aldol condensation reaction to produce the TBDOPV comonomer and a Stille polymerisation to bridge the TBDOPV unit with the thiophene unit (Fig. 1e). Thus, **5** is characterised by a different chemistry of the backbone, by a lower side chain attachment density with respect to **1**-**3** and by even longer and more flexible branched alkyl side chains when compared with **1**, **2** and **4**.

No sequence defects of the type described for **2** and **3** were ever observed within the TBDOPV monomer (Figs. 5c and 5d). Similar to the case of **4,** this is due to the incorporation of the lactone-based moiety which does not allow the effective exchange reactions described in Fig. 3b. However, high-resolution STM images (Fig. 5d and Fig. S16) show that kinks are still present, caused by "wrong" couplings, with the corresponding reaction pathways explained in Fig. S15. This finding demonstrates that this type of coupling defects is not limited to polymerisation reactions, as is seen in the case of polymers **1**-**4**, but can also occur during the synthesis of small molecules, as seen with polymer **5**. This crucially underscores that these defects are intrinsic to the aldol condensation reaction itself. Actual polymerisation defects were observed for **5** too, but these were homocoupling defects generated during the Stille reaction cycle both between TBDOPV and thiophene comonomers (see section 3.6 of the SI for more details)[25,30].

Conclusions

In this work, we have employed the ESD-STM technique to precisely characterise the chemical structure of four *n*-type co-polymers of increasing complexity (**2-5**), all synthesised via aldol condensation. The high-resolution STM images provide unprecedented insights into the microstructure of these conjugated polymers, revealing the presence of so-far unaccounted defects in the backbones of all four polymers. These defects manifest as deviations from the expected polymer sequence (sequence defects) and as kinks in the backbone structure (coupling defects). A quantitative analysis unveils a non-negligible number of defects in both the polymers and the small molecules synthesised by aldol condensation. These findings strongly imply that both types of defects are intrinsic to the aldol condensation reaction itself and highlight that the actual structure of the synthesised molecules can significantly deviate from the expected "ideal" structure. Moreover, it is found that, while coupling defects depend only weakly on the chemical nature and bulkiness of the side chains, these latter have a significant influence on the sequence defects.

Based on the experimental results, detailed reaction pathways elucidating the formation of the observed defects are proposed. These include, for the coupling defects, reactions occurring at alternative coupling sites of the comonomers both in *trans* and *cis* configurations, and, for the sequence defects, an acid catalysed hydride transfer reaction causing a functional group interconversion between comonomers. Our analysis also shows that sequence defects do not occur in **4** and **5** since the incorporation of side chain-free lactone-based comonomers effectively quenches functional group exchange reactions.

The results of this work bring new insight into the mechanism of the aldol condensation reaction and offer a rational basis for future design and improvement of new polymerisation methods to better control the polymer structure and thus their performance in opto-electronic applications. Moreover, this study demonstrates the prevalence and drastic impact of defects on the sequence and structure of conjugated polymers made by aldol condensation and highlights that care should be taken when assuming a perfect alternating repeating sequence of comonomers arranged in a straight, all-*trans* configuration. Future work should aim to optimise reaction conditions and monomer composition to deter and hopefully eliminate the unwanted defects. This would eventually fully realise the promise of the aldol condensation reaction as a much greener and

sustainable alternative to current synthetic strategies for conjugated polymers, with no toxic byproducts and without the requirement of expensive rare metal catalysts.

Methods

Materials

The synthetic details for polymers **1-2** are described by Onwubiko et al., (38) and those for polymers **3-5** by Marks et al., (40) Alsufyani et al. (24) and Lu et al. (41), respectively. The polymers analysed in this work were synthesised according to these protocols.

STM characterisation

The STM experiments were performed in an ultra-high vacuum (UHV) low temperature (LT) STM system (CreaTec Fischer & Co. GmbH). Atomically clean and flat Au(111) surfaces were prepared by cycles of Ar^+ ion sputtering ($p_{Ar^+} = 1.0 \times 10^{-5}$ mbar, 10 min) and annealing (400 °C, 10 min) and were checked by STM before being exposed to the polymers. All polymers were initially dissolved in chlorobenzene at the same concentration (0.05 mg/ml) and sonicated for 20 min (or longer if necessary) to ensure the molecules dissolved completely. Then 1.7 ml of dissolved polymer solution was mixed with 0.3 ml of methanol, and the mixture was deposited by ESD (Molecularspray Ltd.) onto the pristine Au(111) surface held at room temperature. After deposition, the sample was cooled down by a liquid nitrogen flow cryostat and transferred to the STM analysis chamber for *in situ* imaging under UHV at low temperature (–196 °C in a bath cryostat). All the STM images were acquired in constant current mode and analysed by WSxM[44]. LMAPper[45] was used to fit the STM images with scaled molecular models of the polymers which had previously been geometry optimised by the MMFF94 force field in the Avogadro software.

References

1. Skotheim, T.A. & Reynolds, J.R. *Conjugated polymers: processing and applications.* (CRC press, 2006).
2. Reynolds, J.R., Thompson, B.C. & Skotheim, T.A. *Conjugated polymers: properties, processing, and applications.* (CRC press, 2019).

3. Burroughes, J.H. et al. Light-emitting diodes based on conjugated polymers. *Nature* **347**, 539-541 (1990).

4. Guo, X., Baumgarten, M. & Müllen, K. Designing π-conjugated polymers for organic electronics. *Prog. Polym. Sci.* **38**, 1832-1908 (2013).

5. Qiu, Z., Hammer, B.A. & Muellen, K. Conjugated polymers–Problems and promises. *Prog. Polym. Sci.* **100**, 101179 (2020).

6. Miyaura, N. & Suzuki, A. Stereoselective synthesis of arylated (E)-alkenes by the reaction of alk-1-enylboranes with aryl halides in the presence of palladium catalyst. *J. Chem. Soc., Chem. Commun.* **19**, 866-867 (1979).

7. Miyaura, N., Yamada, K. & Suzuki, A. A new stereospecific cross-coupling by the palladium-catalyzed reaction of 1-alkenylboranes with 1-alkenyl or 1-alkynyl halides. *Tetrahedron Lett.* **20**, 3437-3440 (1979).

8. Tsutomu, M., Kunio, M. & Atsumu, O. Arylation of Olefin with Aryl Iodide Catalyzed by Palladium. *Bull. Chem. Soc. Jpn.* **44**, 581-581 (1971).

9. Heck, R.F. & Nolley Jr, J. Palladium-catalyzed vinylic hydrogen substitution reactions with aryl, benzyl, and styryl halides. *J. Org. Chem.* **37**, 2320-2322 (1972).

10. Sonogashira, K., Tohda, Y. & Hagihara, N. A convenient synthesis of acetylenes: catalytic substitutions of acetylenic hydrogen with bromoalkenes, iodoarenes and bromopyridines. *Tetrahedron Lett.* **16**, 4467-4470 (1975).

11. Tamao, K., Sumitani, K. & Kumada, M. Selective carbon-carbon bond formation by cross-coupling of Grignard reagents with organic halides. Catalysis by nickel-phosphine complexes. *J. Am. Chem. Soc.* **94**, 4374-4376 (1972).

12. Milstein, D. & Stille, J. A general, selective, and facile method for ketone synthesis from acid chlorides and organotin compounds catalyzed by palladium. *J. Am. Chem. Soc.* **100**, 3636-3638 (1978).

13. Ran, Y., Guo, Y. & Liu, Y. Organostannane-free polycondensation and eco-friendly processing strategy for the design of semiconducting polymers in transistors. *Mater. Horiz.* **7**, 1955-1970 (2020).

14. Wei, X., Zhang, W. & Yu, G. Semiconducting polymers based on isoindigo and its derivatives: synthetic tactics, structural modifications, and applications. *Adv. Funct. Mater.* **31**, 2010979 (2021).

15. Zhu, X., Duan, J., Chen, J., Liu, R., Qin, Z., Chen, H. & Yue, W. Aldol condensation for the construction of organic functional materials. *Angew. Chem.* **136**, e202311879 (2023).

16. Perrin, C.L. & Chang, K.-L. The complete mechanism of an aldol condensation. *J. Org. Chem.* **81**, 5631-5635 (2016).

17. Mahrwald, R. *Modern Aldol Reactions.* (Wiley Online Library, 2004).

18. Sachs, M. et al. Tracking charge transfer to residual metal clusters in conjugated polymers for photocatalytic hydrogen evolution. *J. Am. Chem. Soc.* **142**, 14574-14587 (2020).

19. Griggs, S. et al. The effect of residual palladium on the performance of organic electrochemical transistors. *Nat. Commun.* **13**, 7964 (2022).

20. Jadhav, T., Fang, Y., Patterson, W., Liu, C.H., Hamzehpoor, E. & Perepichka, D.F. 2D poly (arylene vinylene) covalent organic frameworks via aldol condensation of trimethyltriazine. *Angew. Chem. Int. Ed.* **58**, 13753-13757 (2019).

21. Raston, C.L. & Scott, J.L. Chemoselective, solvent-free aldol condensation reaction. *Green Chem.* **2**, 49-52 (2000).

22. Nielsen, A.T. & Houlihan, W.J. The aldol condensation. *Org. Chem.* **16**, 1-438 (2004).

23. Yu, Y. et al. A novel class of rigid-rod perylene diimides and isoindigo semiconducting polymers. *Polym. Chem.* **13**, 536-544 (2022).

24. Alsufyani, M. et al. Lactone backbone density in rigid electron-deficient semiconducting polymers enabling high n-type organic thermoelectric performance. *Angew. Chem. Int. Ed.* **61**, e202113078 (2022).

25. Vanderspikken, J., Liu, Z., Wu, X. et al. On the importance of chemical precision in organic electronics: fullerene intercalation in perfectly alternating conjugated polymers. *Adv. Funct. Mater.* **33**, 2309403 (2023).

26. Hendriks, K.H., Li, W., Heintges, G.H., van Pruissen, G.W., Wienk, M.M. & Janssen, R.A. Homocoupling defects in diketopyrrolopyrrole-based copolymers and their effect on photovoltaic performance. *J. Am. Chem. Soc.* **136**, 11128-11133 (2014).

27. Lombeck, F. et al. On the effect of prevalent carbazole homocoupling defects on the photovoltaic performance of PCDTBT: $PC_{71}BM$ solar cells. *Adv. Energy Mater.* **6**, 1601232 (2016).

28. Vangerven, T. et al. Molar mass versus polymer solar cell performance: Highlighting the role of homocouplings. *Chem. Mater.* **27**, 3726-3732 (2015).

29. Pirotte, G., Verstappen, P., Vanderzande, D. & Maes, W. On the "true" structure of push–pull-type low-bandgap polymers for organic electronics. *Adv. Electron. Mater.* **4**, 1700481 (2018).

30. Warr, D.A. et al. Sequencing conjugated polymers by eye. *Sci. Adv.* **4**, eaas9543 (2018).

31. Lawton, S.S., Warr, D., Perdigão, L.M., Chang, Y., Pron, A., Costantini, G. & Haddleton, D.M. Determining the sequence and backbone structure of "semi-statistical" copolymers as donor–acceptor polymers in organic solar cells. *Sustain. Energy Fuels.* **4**, 2026-2034 (2020).

32. Ponder Jr, J.F. et al. Low-defect, high molecular weight indacenodithiophene (IDT) polymers via a C–H activation: evaluation of a simpler and greener approach to organic electronic materials. *ACS Mater. Lett.* **3**, 1503-1512 (2021).

33. Moro, S. et al. Molecular-scale imaging enables direct visualization of molecular defects and chain structure of conjugated polymers. *ACS Nano* **18,** 11655-11664 (2024).

34. Chen, H. et al. The effect of ring expansion in thienobenzo[b]indacenodithiophene polymers for organic field-effect transistors. *J. Am. Chem. Soc.* **141**, 18806-18813 (2019).

35. Xiao, M. et al. Anisotropy of charge transport in a uniaxially aligned fused electron-deficient polymer processed by solution shear coating. *Adv. Mater.* **32**, 2000063 (2020).

36. Hallani, R.K. et al. Regiochemistry-driven organic electrochemical transistor performance enhancement in ethylene glycol-functionalized polythiophenes. *J. Am. Chem. Soc.* **143**, 11007-11018 (2021).

37. Moro, S. et al. The effect of glycol side chains on the assembly and microstructure of conjugated polymers. *ACS Nano* **16**, 21303–21314 (2022).

38. Onwubiko A. et al. Fused electron deficient semiconducting polymers for air stable electron transport. *Nat. Commun.* **9**, 416 (2018).

39. Mistry, A. et al. The synthesis and STM/AFM imaging of 'olympicene'benzo [cd] pyrenes. *Chem. Eur. J.* **21**, 2011-2018 (2015).

40. Marks, A., Chen, X. et al. Synthetic nuances to maximize n-type organic electrochemical transistor and thermoelectric performance in fused lactam polymers. *J. Am. Chem. Soc.* **144**, 4642-4656 (2022).

41. Lu, Y. et al. Persistent conjugated backbone and disordered lamellar packing impart polymers with efficient n-doping and high conductivities. *Adv. Mater.* **33**, 2005946 (2021).

42. Yu, Z.-D. et al. High n-type and p-type conductivities and power factors achieved in a single conjugated polymer. *Sci. Adv.* **9**, eadf3495 (2023).

43. Saeedifard, F. et al. Use of a multiple hydride donor to achieve an n-doped polymer with high solvent resistance. *ACS Appl. Mater. Interfaces* **14**, 33598-33605 (2022).

44. Horcas, I., Fernández, R., Gomez-Rodriguez, J., Colchero, J., Gómez-Herrero, J. & Baro, A. WSXM: A software for scanning probe microscopy and a tool for nanotechnology. *Rev. Sci. Instrum.* **78**, 013705 (2007).

45. Perdigão, L.M.A. LMAPper – Where scanning probe microscopy and molecular visualisation meet. *https://sourceforge.net/projects/spm-and-mol-viewer/*.

Acknowledgements

X.W. acknowledges co-funding from the European Union's Horizon 2020 research and innovation Marie Skłodowska-Curie Actions, under grant agreement no. 945380. G.C. and S.M. acknowledge support from a UK – Saudi Challenge Fund grant from the British Council's Going Global Partnerships programme. M.A. and I.M. acknowledge financial support from KAUST Office of Sponsored Research CRG10, by EU Horizon2020 grant agreement n°952911, BOOSTER, grant agreement n°862474, RoLA-FLEX, and grant agreement n°101007084 CITYSOLAR. X.C. would like to acknowledge support from the National Natural Science Foundation of China (Grant NO.22205004), as well as EPSRC Projects EP/T026219/1, EP/W017091/1, and EP/L011972/1.